ACS OMEGA

Open Access

http://pubs.acs.org/journal/acsodf

Article

High-Speed Fluctuation Analysis of Silver-Nanoparticle SERS in Solutions

Kota Uchiyama, Takahiro Kondo, and Yuika Saito*

Cite This: *ACS Omega* 2024, 9, 42950−42956

Read Online

ACCESS | Metrics & More | Article Recommendations | Supporting Information

ABSTRACT: We analyzed the fluctuation of surface-enhanced Raman spectra with a temporal resolution of 25 ms using a conventional electron-multiplying charge-coupled device camera experimental setup. The signal-to-noise ratio of the spectra was improved using density-based spatial cluster analysis with noise. Silver nanoparticles (AgNPs) with different sizes were dispersed as surface-enhanced Raman spectroscopy platforms in violet aqueous solutions. The movement of AgNPs and the fluctuation of the spectra were characterized. The fluctuation (signal ON and OFF) was evaluated on the basis of the time intervals between ON and OFF timing. The behavior of each AgNP solution was explained by a two-dimensional random walk model, which means that the phenomenon was mainly governed by the Brownian motion of the AgNPs in the solution. The fluctuation was also compared among three different Raman modes, one of which showed anomalous behavior.

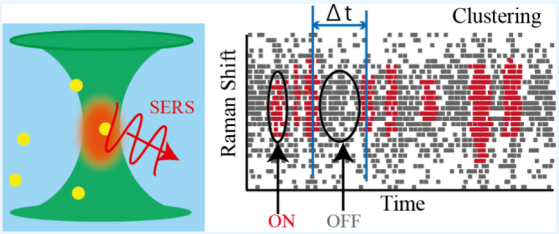

INTRODUCTION

Since its discovery in the 1970s, surface-enhanced Raman spectroscopy (SERS)[1] has been applied in many fields, including analytical chemistry,[2−6] biology,[7,8] and high-resolution microscopy.[9] In addition to its advantage of extremely high signal enhancement,[1] SERS demonstrates a temporal fluctuation phenomenon.[10] The origin of the SERS fluctuation can be categorized into three effects: (1) the movement of molecules around the SERS-active spots via environmental interactions such as temperature or solvent flow,[11−17] (2) the movement of metal nanoparticles or nanostructures, including aggregation configurations and Brownian motions,[18−23] and (3) the fluctuation of surface plasmon polaritons, which leads to modulation of the resonance Raman effect of the molecules via vibronic coupling.[24−27] In many cases, fluctuation is governed by a combination of these effects. SERS fluctuation is thus a complex phenomenon that depends on both the sample as well as environmental factors; it has therefore been observed in a wide range of time scales from seconds to nanoseconds.[28]

The temporal resolution is selected on the basis of the system being observed. If we are interested in investigating the movement of nanoparticles and spectroscopic fluctuations simultaneously, then a temporal resolution on the order of ∼10 ms is needed. To trace an event at high temporal resolutions, a point detector such as an avalanche photodiode[14] can be employed at the expense of spectroscopic information. An electron-multiplying charge-coupled device (EMCCD) camera can achieve a temporal resolution on the order of 10 ms; however, multiplex detection using a diffraction grating lowers the signal-to-noise (SN) ratio, and increasing the electronic gain causes shot noise. Thus, attention is needed to separate the signal from the noise in high-speed spectroscopic measurements. Even though the signal with the highest intensity is to be extracted, it is highly probable that the signal is shot noise when the SN ratio is poor. To extract a signal from low-SN data, the intensity and wavelength axes should be considered simultaneously. Density-based spatial clustering analysis with noise (DBSCAN) is a method to search high-density areas in a multidimensional space and can therefore be used to separate signals from noise in Raman spectra.[29,30]

In this work, we conducted a temporal fluctuation analysis of SERS spectra in solutions with a temporal resolution of 25 ms. The samples were crystal violet aqueous solutions containing silver nanoparticles (AgNPs) for SERS enhancement. We used isolated metal nanoparticles in solution because they are often used to track biological events.[31,32] We discuss both the movement of the nanoparticles and the acquired SERS spectra. Because of the improvement of the SN using DBSCAN analysis, the accumulation time was as short as 10 ms. The signal fluctuation was measured for AgNPs with different sizes, and the results were compared to the predictions of a two-dimensional random walk model. The temporal behavior for different Raman peaks is also discussed.

Received: June 22, 2024
Revised: September 2, 2024
Accepted: October 3, 2024
Published: October 10, 2024

https://doi.org/10.1021/acsomega.4c05817
ACS Omega 2024, 9, 42950−42956

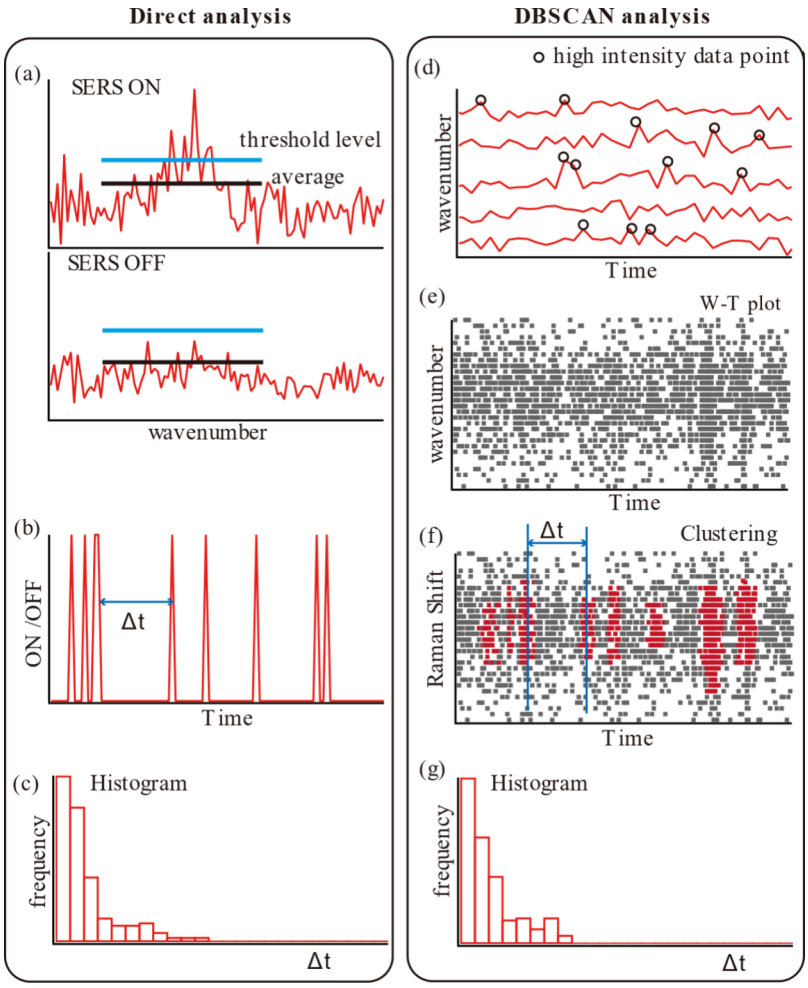

Figure 1. Process of temporal fluctuation analysis by direct and DBSCAN analysis, (a) threshold level determination, (b) definition of Δt, (c) the histogram of Δt obtained by direct analysis, (d) selection of high-intensity data points for DBSCAN, (e) time-wavenumber (T-W) plot, (f) Δt obtained by DBSCAN process, (g) the histogram of Δt obtained by DBSCAN analysis.

METHODS

The temporal fluctuation of SERS was characterized by using ON and OFF states. When the signal SN ratio was sufficiently high, we determined ON and OFF states directly from the spectra by setting a threshold level. However, when the SN ratio was poor, especially in high-temporal-resolution measurements, DBSCAN analysis was necessary. Figure 1 shows a schematic of the data analysis. We performed two data analyses: direct analysis and DBSCAN analysis. The direct analysis was valid only for the data with a good SN ratio, where the ON and OFF states were determined directly from spectra (Figure 1(a)). The threshold level was empirically determined as $I_{ave} + 0.5\sigma$, where I_{ave} is the average peak height and σ is the standard deviation for all of the collected spectra. Fluctuation was evaluated by the time interval (Δt) between a nearest ON state indicated in Figure 1(b). The relation between Δt and its frequency are shown in a histogram in Figure 1(c) to evaluate the temporal behavior of SERS. We used the result of direct analysis as the "reference" to determine the DBSCAN parameters, as discussed in the Results section. In the DBSCAN analysis, the ON and OFF states were determined by a clustering process. First, as shown in Figure 1(d), high-intensity data points ($>I_{ave} + 0.5\sigma$) in the time domain were selected for each wavenumber. Second, the selected data points were plotted on a two-dimensional graph called a time–wavenumber (T–W) plot (Figure 1(e)). The time axis in the T–W space was adjusted by multiplying by a factor (the time ratio) because the time and wavenumber axes have different units. We set time_ratio = 100 in this case. Third, the DBSCAN process was applied to the T–W. The clusters were classified into ON states, whereas other data points were classified into OFF states (Figure 1(f)). Parameter Δt was the distance between the centroid of a nearest cluster pair, as indicated in Figure 1(f). The relation between Δt and its frequency is again shown in a histogram (Figure 1(g)). The DBSCAN process requires two parameters: eps (the distance from a particular data point) and min_samples (minimum number of sample points to be a cluster), which were determined by using the direct analysis results. The values we used were eps = 100 and min_samples = 16 or 17. The values of min_samples are shown in Table S1.

We obtained SERS spectra using a 532 nm continuous-wave laser with a power of 23 mW at the exit of a beam expander. The diameter of the laser beam was expanded 10-fold by the beam expander to cover the pupil plane of an objective lens. We placed the shutter in front of the expander to minimize any optical damage to the sample. The measurements were performed on an inverted microscope (TE2000-U, Nikon) equipped with an objective lens (60× , NA 0.7). The signal passed through an edg filter and was introduced into a

https://doi.org/10.1021/acsomega.4c05817
ACS Omega 2024, 9, 42950−42956

spectrometer (Acton, SpectraPro 2300i, slit width of 100 μm). The spectra were acquired by an EMCCD camera (ProEM, Princeton Instruments, EM gain set to 30). For high-SN measurements, 3600 SERS spectra were acquired with an accumulation time of 1000 ms. For high-temporal-resolution measurements, 10,000 SERS spectra were acquired with an accumulation time of 10 ms. Because of the data transfer speed of the EMCCD camera, the net temporal resolution was 25 ms. DBSCAN proceed by ~3000 spectra; 10000 is a good number of spectra to claim the reliability and the generalizability of the results. The net measurement time was 100 s, which was again a reasonable duration to evaluate SERS fluctuation.

Mixed aqueous solutions of crystal violet (CV; 5×10^{-7} mol/L) with AgNPs were prepared. AgNPs with diameters of 10, 20, 30, 40, and 60 nm were used as the SERS platforms. The concentration of AgNPs was 0.02 mg/mL irrespective of the AgNP particle size; therefore, the amount of Ag was the same for all of the samples, whereas the particle density was different. The concentration and size distribution of AgNPs are summarized in Figure S2. Assuming that the laser focus was diffraction limited sphere, the number of CV molecules within the focus was 15, some of which would meet a AgNP giving intense SERS signals. According to the UV−vis absorption spectra in Figure S3, there is no sign of NP aggregates in our sample; therefore, we considered that all AgNPs are a single NP.

The fluctuation was modeled using a two-dimensional random walk model of AgNPs in a solution. The calculation model is shown in Figure 2. In this model, AgNPs move

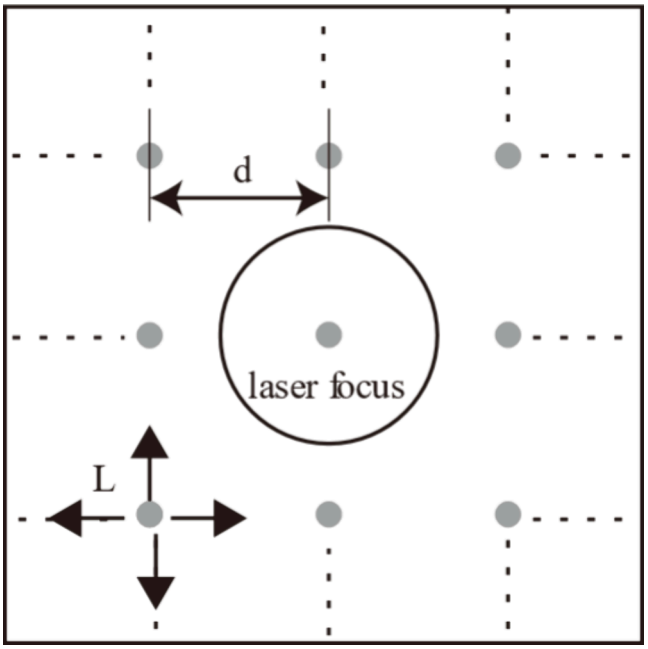

Figure 2. Initial configuration of the two-dimensional random walk model (gray circles: AgNPs; d: AgNP distance; L: simulation step).

stepwise in either the right, left, up, or down direction randomly. SERS enhancement occurs when one or a few (defined as parameter B) AgNPs enter the focal spot of the laser. The initial AgNP distance d was determined by the particle density. The simulation step was determined by the diffusion constant of AgNPs in 25 °C water, and the measurement interval was 25 ms. The diameter of the laser spot was 463 nm, as calculated on the basis of the wavelength and the diffraction limit of the objective lens. The simulation area was set to 200 × d nm; when a particle reached the boundary, it re-entered at the opposite coordinate. The random walk simulation was repeated 40,000 times. The simulation step was was four times as much as the spectral set of SERS measurements. Table 1 shows the parameters used for the random walk model.

Table 1. Parameters of the two-dimensional random walk simulation[a]

Size (nm)	B	d (nm)	D	L (nm)
10	3	794	4.90×10^{-11}	2280
20	2	1478	2.45×10^{-11}	1612
30	1	2462	1.63×10^{-11}	1317
40	1	2974	1.22×10^{-11}	1140
60	1	4900	8.17×10^{-12}	930.9

[a]B: threshold number of AgNPs in the laser focal spot giving the SERS ON state; d: distance between AgNPs in the initial configuration; D: diffusion constant; L: simulation step where t = 25 ms.

RESULTS AND DISCUSSION

The DBSCAN parameters were determined to reproduce the result of direct analysis as much as possible. The histograms of fluctuation by the direct analysis are shown in Figure S1A. Using the result of the direct analysis as the reference, we performed a DBSCAN analysis. In addition to the concordance in the temporal axis, the number of cluster formations was another important indicator to determine the eps and the min_samples. The validity of these parameters is shown in S1B, where the similarity between the reference results and the DBSCAN results is obvious. The parameter min_samples was determined by the total number of clusters, which should be equal to the number of ON times in the direct analysis. Table S3 shows the comparison between the direct analysis and the DBSCAN analysis. The result obtained by the DBSCAN analysis was almost identical to the results counted directly. Eps, on the other hand, was determined by the time ratio when we construct the T-W. In the cluster formation, eps influences the shape of the cluster. If eps < time_ratio, clusters did not extend in the direction of the wavenumber axis and therefore failed to cover a single Raman band. On the other hand, if eps > time_ratio, the cluster extends in the wavelength axis, while little change was observed in the temporal axis (see Figure S4). We employed DBSCAN analysis for higher temporal measurements using the same eps and the min_samples.

Figure 3 shows histograms of the temporal SERS behavior for three Raman peaks (914, 1181, and 1622 cm^{-1}) and for AgNPs with five different particle sizes (10, 20, 30, 40, and 60 nm). First, we focus on the peak at 1622 cm^{-1} in Figure 2(a). The ON time interval Δt is maximal at the shortest period and gradually decreases as the interval increases in most of the samples. Events at longer time intervals were also observed for small AgNPs (e.g., 10 and 20 nm). The decay in the histograms was the fastest for the 40 nm AgNPs; the decay then slowed in the 60 nm AgNP sample. The results in Figure 3 are partially explained by a random walk model. We assume that SERS enhancement occurred when a AgNP migrates into the laser focal spot via Brownian motion. The simulation was carried out for a two-dimensional random walk model of

https://doi.org/10.1021/acsomega.4c05817
ACS Omega 2024, 9, 42950−42956

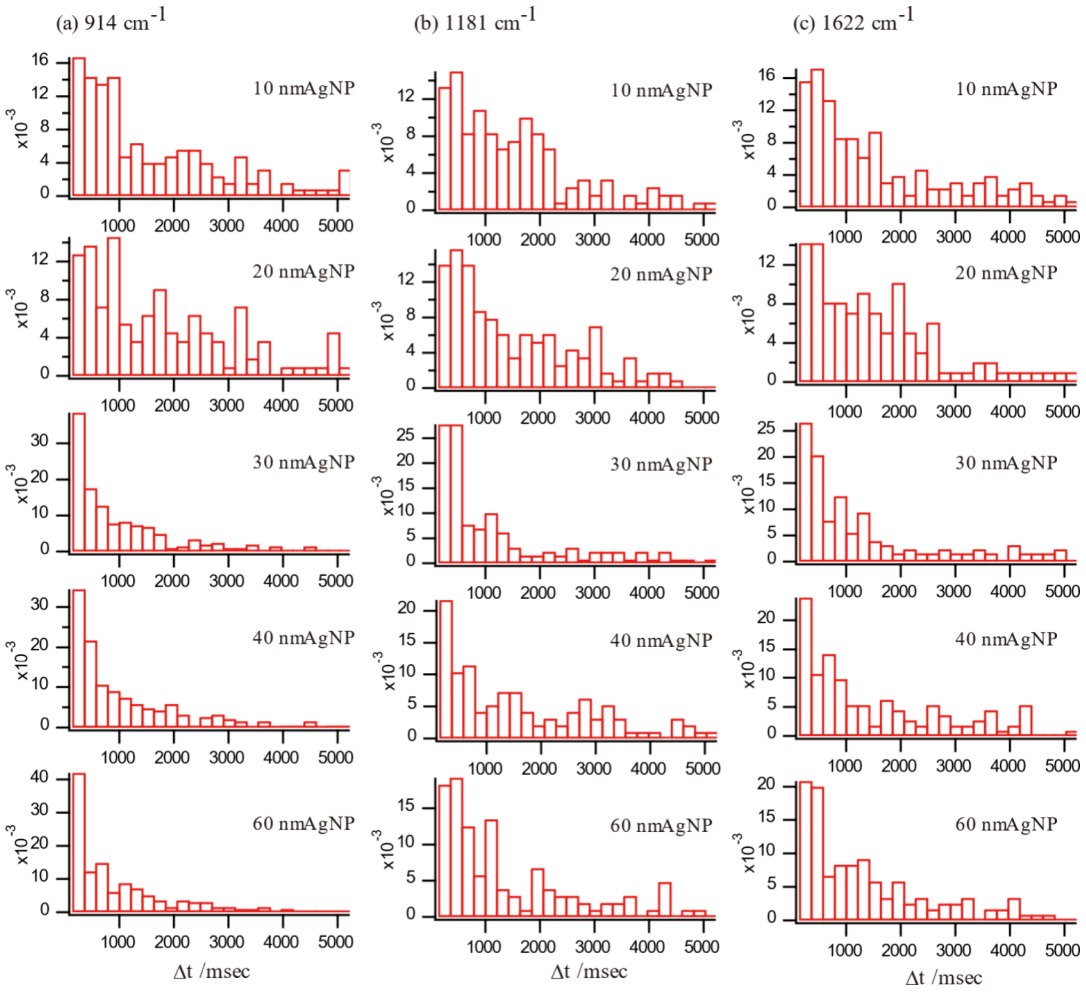

Figure 3. Histograms of Δt obtained by DBSCAN; SERS spectra were acquired with a 10 ms accumulation time: (a) 914 cm^{-1}, (b) 1181 cm^{-1}, and (c) 1622 cm^{-1} Raman modes. AgNPs with diameters of 10, 20, 30, 40, and 60 nm were used.

AgNPs moving in and out of a laser spot. Because the number of AgNPs was substantially smaller than the number of CV molecules, the rate was governed by the AgNPs. Figure 4 shows the results of the random walk simulations for each AgNP particle size. The decay in the histograms in Figure 4 shows a size dependence similar to the experimental results. However, in Figure 3, the decay is fastest for the 40 nm AgNPs and slows for the 60 nm AgNP sample, which was not reproduced by the simulation.

According to Mie theory, ~40 nm is the largest limit of the dipole approximation of a AgNP, and, empirically, the SERS enhancement is also maximal in this size range.[1,33] The mismatch of this simplified threshold setting is the main cause of the difference between the experimental and the simulation results. As shown in Figure S2, a random walk histogram was also influenced by parameter B (i.e., the threshold number of nanoparticles in the laser focal spot that gives the SERS ON state). As indicated in Table 1, parameter B was set to 3 for 10 nm AgNPs, 2 for 20 nm AgNPs, and 1 for the rest of the AgNPs because the enhancement efficiency of each AgNP sample differs depending on the AgNP particle size. Another reason for the observed difference is that the simulation was conducted in two dimensions, because of the limitations of the computation source. The experimental system was 3D, and the movement of nanoparticles was also affected by gravity. Given the slight difference between the results in Figures 2 and 3, we reasonably concluded that the temporal SERS fluctuation originated predominantly from the motion of the AgNPs. We add that according to Table S2, the size distribution was in the range of 12% ~ 18% for all AgNP samples. Therefore, we think that the size distribution was not the essential reason for the difference in fluctuation behavior seen in different samples in Figure 3.

Considering a computational resource, a two-dimensional model was a realistic choice. Since we could reproduce the histograms in Figure 3 quite well even by the two-dimensional model, we believe that the random walk model is suitable for explaining the phenomena. In a three-dimensional model, the procedure was basically the same, but replacing average migration length $L = \sqrt{4Dt}$ to $\sqrt{6Dt}$. We can safely neglect the effect of gravity because the sedimentation speed under 9.8 ms^{-2} for 60 nm AgNP is 20 nm/s, which is much slower than L (5887 nm for 1 s). The Random walk model was not the perfect one to describe the fluctuation; there would be other factors such as fluid flow, system instability, etc. which we did not consider for simplicity.

Next, we discuss the temporal behavior of different Raman modes. The temporal behavior of different Raman modes is expected to be identical when all of the Raman peaks are equally enhanced. Figure 3 shows the temporal behavior of three Raman modes: (a) 914 cm^{-1}: an out-of-plane mode,

https://doi.org/10.1021/acsomega.4c05817
ACS Omega 2024, 9, 42950−42956

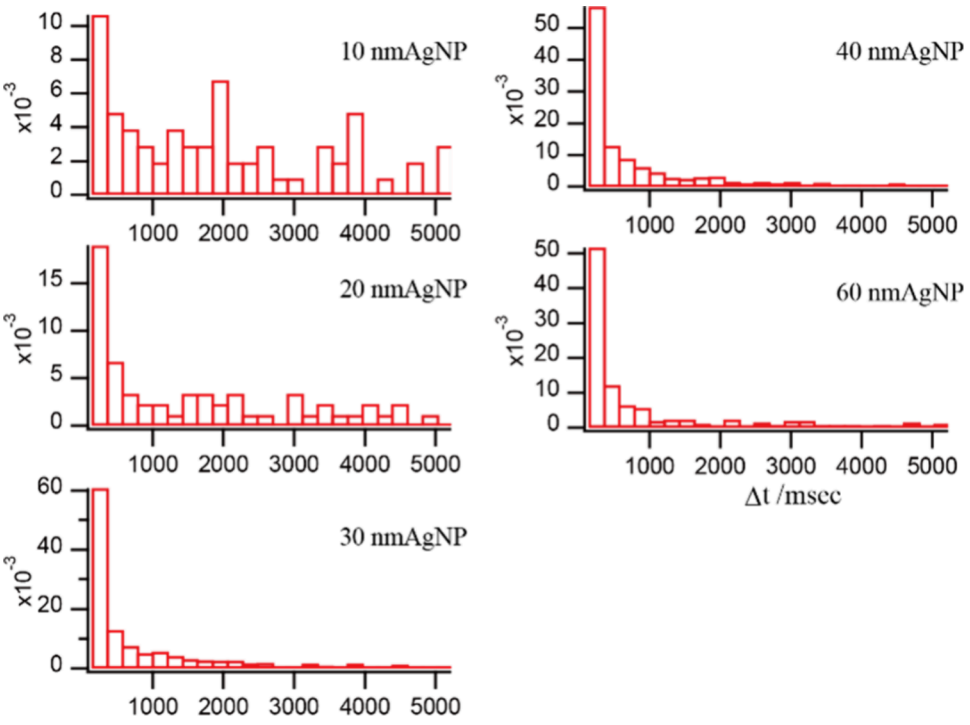

Figure 4. Histogram of Δt values obtained by the two-dimensional random walk model simulation. AgNPs with diameters of 10, 20, 30, 40, and 60 nm were used.

benzene mode 17a, (b) 1181 cm^{-1}: an in-plane mode, benzene mode 9a, and (c) 1622 cm^{-1}: the in-plane mode, benzene mode 8a.[34−37] The temporal behaviors of the 914 and 1622 cm^{-1} modes are similar; however, the behavior differs for the 1181 cm^{-1} mode, especially in the spectra of the 40 nm AgNP sample having the second peak around 3000 ms. As noted in our discussion of the random walk model, the histogram was influenced by the *B* parameter, meaning that the signal intensity of a single event should be considered. Therefore, we expected the 1181 cm^{-1} mode to benefit less from SERS enhancement compared with the other two modes. Figure 5 shows the SERS (with 60 nm AgNPs) and Raman (without AgNPs) spectra of CV. In the normal Raman spectrum; two peaks are observed at 1174 and 1193 cm^{-1}. By contrast, in the SERS spectrum, only one peak is observed at 1181 cm^{-1}. On the basis of previous work,[34,35] the higher-frequency peak is assigned to a doubly degenerate E mode, whereas the lower-frequency peak is assigned to a totally symmetric A_1 mode. If the Raman frequency of the higher-frequency mode is downshifted and the lower-frequency mode is less affected, then the spectral shape would resemble a single peak, because the resonance Raman process governing A- or B-type resonance depends on the vibrational symmetry. The doubly degenerate E mode has been reported to be preferentially enhanced by SERS because of the Herzberg−Teller surface selection rules.[37] The downshift of the frequency means that the mode is influenced by the adsorption of CV molecules. A CV molecule has two Raman-active modes at ∼1181 cm^{-1}; one mode is influenced by SERS and the other is less influenced, resulting in peaks that coexist at almost identical frequencies. The anomalous behavior of the 1181 cm^{-1} mode can thus be explained by the SERS efficiency.

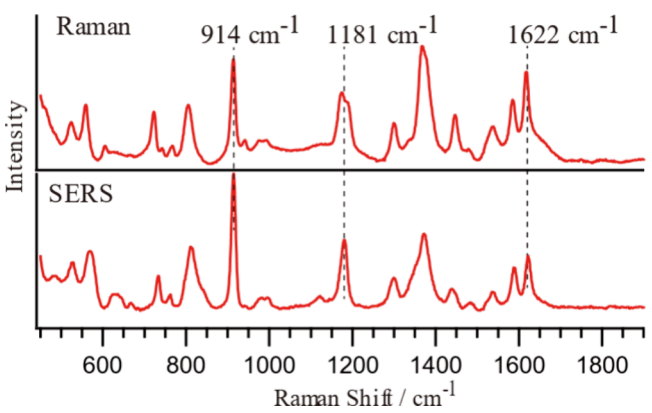

Figure 5. SERS (60 nm AgNPs) and Raman spectra of CV aqueous solutions. A peak shift and broadening were observed for the 1181 cm^{-1} mode.

CONCLUSIONS

We evaluated the temporal fluctuation of the SERS spectra of CV dissolved in AgNP-containing aqueous solutions with 25 ms temporal resolution. AgNPs with particle diameters of 10, 20, 30, 40, and 60 nm were used as SERS platforms. DBSCAN analysis helped to improve the SN ratio of the spectra, which were otherwise difficult to categorize as corresponding to the ON or OFF state. The ON and OFF fluctuations were discussed on the basis of the interval between the ON times (Δt) and were presented in a histogram. The nanoparticle-size-dependent temporal behavior was explained well by a two-dimensional random walk model; therefore, the fluctuation was mainly due to Brownian motion of the AgNPs. The characteristics of the histogram were also influenced by the particle size, density, and SERS efficiency of each nanoparticle sample.

We also compared and discussed the differences in the temporal behaviors for the three different Raman modes. The

https://doi.org/10.1021/acsomega.4c05817
ACS Omega 2024, 9, 42950−42956

size-dependent fluctuation was similar for two of the modes; only the 1181 cm^{-1} mode showed a difference. These results were attributed to the 1181 cm^{-1} mode being the summation of two closely overlapped modes with different vibrational symmetry, where one mode was strongly affected and the other was weakly affected by SERS. Therefore, the net SERS enhancement of the 1181 cm^{-1} mode was weaker than the enhancements of the other modes.

We successfully evaluated the movement of nanoparticles and a molecular system in a solution simultaneously through SERS-based temporal behavior analysis. We expect our findings to contribute to analytical and biological applications of nanoparticle-based SERS.

■ ASSOCIATED CONTENT

Supporting Information

The Supporting Information is available free of charge at https://pubs.acs.org/doi/10.1021/acsomega.4c05817.

DBSCAN parameter evaluation and sample information; Table S1:Minimum number of sample points to be a cluster, Table S2: The concentration and the size distribution of AgNPs, Table S3: Number of Clusters formed in DBSCAN analysis, Figure S1A: Histogram of the Δt values obtained by direct analysis, Figure S1B: Histogram of the Δt values obtained by DBSCAN, Figure S2: Histogram of the Δt values obtained by the two-dimensional random walk model, Figure S3: UV−vis absorption spectra of isolated AgNPs and aggregated AgNPs, Figure S4: Eps dependence of cluster formation (PDF)

■ AUTHOR INFORMATION

Corresponding Author

Yuika Saito − *Department of Chemistry, Gakushuin University, Toshima, Tokyo 171-8588, Japan;* orcid.org/0000-0002-7003-157X; Email: yuika.saito@gakushuin.ac.jp

Authors

Kota Uchiyama − *Department of Chemistry, Gakushuin University, Toshima, Tokyo 171-8588, Japan*

Takahiro Kondo − *Department of Chemistry, Gakushuin University, Toshima, Tokyo 171-8588, Japan;* orcid.org/0000-0001-7398-4117

Complete contact information is available at: https://pubs.acs.org/10.1021/acsomega.4c05817

Notes

The authors declare no competing financial interest.

■ ACKNOWLEDGMENTS

This work was supported by JSPS KAKENHI (grant nos. 20K15130, 21K04810, and 24K08205).

■ REFERENCES

(1) Moskovits, M. Surface enhanced Raman Spectroscopy. *Rev. Mod. Phys.* **1985**, *57*, 783−826.

(2) Zhang, Y.; Chu, W.; Foroushani, A. D.; Wang, H.; Li, D.; Liu, J.; Barrow, C. J.; Wang, X.; Yang, W. New Gold Nanostructures for Sensor Applications: A Review. *Materials* **2014**, *7*, 5169−5201.

(3) Yamamoto, Y. S.; Ozaki, Y.; Itoh, T. Recent progress and frontiers in the electromagnetic mechanism of surface-enhanced Raman scattering. *J. Photochem. Photobiology C: Photochem. Rev.* **2014**, *21*, 81−104.

(4) Li, C.; Xu, S.; Yu, J.; Li, Z.; Li, W.; Wang, J.; Liu, A.; Man, B.; Yang, S.; Zhang, C. Local hot charge density regulation: Vibration-free pyroelectric nanogenerator for effectively enhancing catalysis and in-situ surface enhanced Raman scattering monitoring. *Nano Energy* **2021**, *81*, No. 105585.

(5) Tian, M.; Wang, J.; Li, C.; Wang, Z.; Liu, G.; Lv, E.; Zhao, X.; Li, Z.; Cao, D.; Liu, H.; Zhang, C.; Xu, S.; Man, B. Qualitative and quantitative detection of microcystin-LR based on SERS-FET dual-mode biosensor. *Biosens. Bioele.* **2022**, *212*, No. 114434.

(6) Li, C.; Man, B.; Zhang, C.; Yu, J.; Liu, G.; Tian, M.; Li, Z.; Zhao, X.; Wang, Z.; Cui, W.; Wang, T.; Wang, J.; Lin, X.; Xu, S. Strong plasmon resonance coupling in micro-extraction SERS membrane for in situ detection of molecular aqueous solutions. *Sens. Act. B Chem.* **2024**, *398*, No. 134767.

(7) Li, P.; Long, F.; Chen, W.; Chen, J.; Chu, P. K.; Wang, H. Fundamentals and applications of surface-enhanced Raman spectroscopy−based biosensors. *Curr. Opinion Biomed. Eng.* **2020**, *13*, 51−59.

(8) Palonpon, A. F.; Ando, J.; Yamakoshi, H.; Dodo, K.; Sodeoka, M.; Kawata, S.; Fujita, K. Raman and SERS microscopy for molecular imaging of live cells. *Nat. protocols* **2013**, *8*, 677−692.

(9) Saito, Y.; Verma, P. Imaging and spectroscopy through plasmonic nano-probe. *Eur. Phys. J. Appl. Phys.* **2009**, *46*, 20101.

(10) Kneipp, K.; Wang, Y.; Kneipp, H.; Perelman, L. T.; Itzkan, I.; Dasari, R. R.; Feld, M. S. Single Molecule Detection Using Surface-Enhanced Raman Scattering (SERS). *Phys. Rev. Lett.* **1997**, *78*, 1667−1670.

(11) Maruyama, Y.; Ishikawa, M.; Futamata, M. Thermal Activation of Blinking in SERS Signal. *J. Phys. Chem. B* **2004**, *108*, 673−678.

(12) Emory, S. R.; Jensen, R. A.; Wenda, T.; Han, M.; Nie, S. Re-examining the origins of spectral blinking in single-molecule and single-nanoparticle SERS. *Faraday Discuss.* **2006**, *132*, 249−259.

(13) Etchegoin, P. G.; Meyer, M.; Blackie, E.; Le Ru, E. C. Statistics of Single-Molecule Surface Enhanced Raman Scattering Signals: Fluctuation Analysis with Multiple Analyte Techniques. *Anal. Chem.* **2007**, *79*, 8411−8415.

(14) Mezni, A.; Dammak, T.; Fkiri, A.; Mlayah, A.; Abid, Y.; Smiri, L. S. Photochemistry at the Surface of Gold Nanoprisms from Surface-Enhanced Raman Scattering Blinking. *J. Phys. Chem. C* **2014**, *118*, 17956−17967.

(15) Kitahama, Y.; Araki, D.; Yamamoto, Y. S.; Itoh, T.; Ozaki, Y. Different behaviour of molecules in dark SERS state on colloidal Ag nanoparticles estimated by truncated power law analysis of blinking SERS. *Phys. Chem. Chem. Phys.* **2015**, *17*, 21204−21210.

(16) Zrimsek, A. B.; Wong, N. L.; Van Duyne, R. P. Single Molecule Surface-Enhanced Raman Spectroscopy: A Critical Analysis of the Bianalyte versus Isotopologue Proof. *J. Phys. Chem. C* **2016**, *120*, 5133−5142.

(17) Magalhaes, F. B.; Jaimes, R. F. V. V.; Corio, P.; Salcedo, W. J. SERS fluctuations of NAD molecules adsorbed on arrays of Au nanocylinders. *Opt. Mater. Ex.* **2021**, *11*, 3154−3177.

(18) Wark, A. W.; Stokes, R. J.; Darby, S. B.; Smith, W. E.; Graham, D. Dynamic Imaging Analysis of SERS-Active Nanoparticle Clusters in Suspension. *J. Phys. Chem. C* **2010**, *114*, 18115−18120.

(19) Barbara, A.; Dubois, F.; Ibanez, A.; Eng, L. M.; Quémerais, P. SERS Correlation Spectroscopy of Silver Aggregates in Colloidal Suspension: Quantitative Sizing Down to a Single Nanoparticle. *J. Phys. Chem. C* **2014**, *118*, 17922−17931.

(20) Patra, P. P.; Chikkaraddy, R.; Tripathi, R. P. N.; Dasgupta, A. V.; Kumar, G. V. P. Plasmofluidic single-molecule surface-enhanced Raman scattering from dynamic assembly of plasmonic nanoparticles. *Nat. Commun.* **2014**, *5*, 4357.

(21) Zhang, F.; Oiticica, P. R. A.; Abad-Arredondo, J.; Arai, M. S.; Oliveira, O. N.; Jaque, D.; Fernandez Dominguez, A. I.; de Camargo, A. S. S.; Haro-Gonzalez, P. Brownian Motion Governs the Plasmonic Enhancement of Colloidal Upconverting Nanoparticles. *Nano Lett.* **2024**, *24*, 3785−3792.

(22) Zhang, D.; Tang, L.; Chen, J.; Tang, Z.; Liang, P.; Huang, Y.; Cao, M.; Zou, M.; Ni, D.; Chen, J.; Yu, Z.; Jin, S. Controllable Self-Assembly of SERS Hotspots in Liquid Environment. *Langmuir* **2021**, *37*, 939−948.
(23) Lindquist, N. C.; Bido, A. T.; Brolo, A. G. Single-Molecule SERS Hotspot Dynamics in Both Dry and Aqueous Environments. *J. Phys. Chem. C* **2022**, *126*, 7117−7126.
(24) Bizzarri, A. R.; Cannistraro, S. Le′vy Statistics of Vibrational Mode Fluctuations of Single Molecules from Surface-Enhanced Raman Scattering. *Phys. Rev. Lett.* **2005**, *94*, No. 068303.
(25) Bizzarri, A. R.; Cannistraro, S. Statistical analysis of intensity fluctuations in single molecule SERS spectra. *Phys. Chem. Chem. Phys.* **2007**, *9*, 5315−5319.
(26) Lombardi, J. R.; Birke, R. L.; Haran, G. Single Molecule SERS Spectral Blinking and Vibronic Coupling. *J. Phys. Chem. C* **2011**, *115*, 4540−4545.
(27) Ma, H.; Chen, Y.; Wang, H.; Wang, X.; Zhang, X.; Han, X.; He, C.; Zhao, B. Charge-Transfer Effect on Surface-Enhanced Raman Spectroscopy in Ag/PTCA: Herzberg−Teller Selection Rules. *J. Phys. Chem. C* **2017**, *121*, 25788−25794.
(28) Lindquist, N. C.; de Albuquerque, C. D. L.; Sobral-Filho, R. G.; Paci, I.; Brolo, A. G. High-speed imaging of surface-enhanced Raman scattering fluctuations from individual Nanoparticles. *Nat. Nanotechnol.* **2019**, *14*, 981−987.
(29) Campello, R. J. G. B.; Moulavi, D.; Sander, J. Density-Based Clustering Based on Hierarchical Density Estimates. *Lecture notes in computer science* **2013**, *7819*, 160−172.
(30) Kondo, T.; Saito, Y. Single-Pulsed SERS with Density-Based Clustering Analysis. *J. Phys. Chem. A* **2022**, *126*, 1755−1760.
(31) Hirano, K.; Ishido, T.; Yamamoto, Y. S.; Murase, N.; Ichikawa, M.; Yoshikawa, K.; Baba, Y.; Itoh, T. Plasmonic Imaging of Brownian Motion of Single DNA Molecules Spontaneously Binding to Ag Nanoparticles. *Nano Lett.* **2013**, *13*, 1877−1882.
(32) Ando, J.; Fujita, K.; Smith, N. I.; Kawata, S. Dynamic SERS Imaging of Cellular Transport Pathways with Endocytosed Gold Nanoparticles. *Nano Lett.* **2011**, *11*, 5344−5348.
(33) Bohren, C. F.; Huffman, D. R. *Absorption and Scattering of Light by Small Particles*; Wiley International: USA, 1998.
(34) Meng, W.; Hu, F.; Zhang, L. Y.; Jiang, X. H.; Lu, L. D.; Wang, X. SERS and DFT study of crystal violet. *J. Mol. Struct.* **2013**, *1035*, 326−331.
(35) Canamares, M. V.; Chenal, C.; Birke, R. L.; Lombardi, J. R. DFT, SERS, and Single-Molecule SERS of Crystal Violet. *J. Phys. Chem. C* **2008**, *112*, 20295−20300.
(36) Angeloni, L.; Smulevich, G.; Marzocchi, M. P. Resonance Raman Spectrum of Crystal Violet. *J. Raman Spectrosc.* **1979**, *8*, 305−310.
(37) Prakash, O. Excitation wavelength-dependent SERS and DFT study to probe Herzberg−Teller selection rules on charge-transfer effect. *J. Chem. Phys.* **2020**, *153*, No. 104703.

https://doi.org/10.1021/acsomega.4c05817
ACS Omega 2024, 9, 42950−42956